Probing Geometric Excitations of Fractional Quantum Hall States on Quantum Computers

Ammar Kirmani[®], ^{1,2} Kieran Bull, ³ Chang-Yu Hou[®], ⁴ Vedika Saravanan, ⁵ Samah Mohamed Saeed, ⁵

Zlatko Papić, ³ Armin Rahmani, ^{6,7} and Pouyan Ghaemi[®], ^{2,8}

¹Department of Physics and Astronomy, Western Washington University, Bellingham, Washington 98225, USA

²Physics Department, City College of the City University of New York, New York, New York 10031, USA

³School of Physics and Astronomy, University of Leeds, Leeds LS2 9JT, United Kingdom

⁴Schlumberger-Doll Research, Cambridge, Massachusetts 02139, USA

⁵Department of Electrical Engineering, City College of the City University of New York, New York, New York 10031, USA

⁶Department of Physics and Astronomy and Advanced Materials Science and Engineering Center,

Western Washington University, Bellingham, Washington 98225, USA

⁷Kavli Institute for Theoretical Physics, University of California, Santa Barbara, California 93106, USA

⁸Graduate Center of the City University of New York, New York, New York 10016, USA

(Received 25 July 2021; revised 27 May 2022; accepted 4 July 2022; published 25 July 2022)

Intermediate-scale quantum technologies provide new opportunities for scientific discovery, yet they also pose the challenge of identifying suitable problems that can take advantage of such devices in spite of their present-day limitations. In solid-state materials, fractional quantum Hall phases continue to attract attention as hosts of emergent geometrical excitations analogous to gravitons, resulting from the nonperturbative interactions between the electrons. However, the direct observation of such excitations remains a challenge. Here, we identify a quasi-one-dimensional model that captures the geometric properties and graviton dynamics of fractional quantum Hall states. We then simulate geometric quench and the subsequent graviton dynamics on the IBM quantum computer using an optimally compiled Trotter circuit with bespoke error mitigation. Moreover, we develop an efficient, optimal-control-based variational quantum algorithm that can efficiently simulate graviton dynamics in larger systems. Our results open a new avenue for studying the emergence of gravitons in a new class of tractable models on the existing quantum hardware.

DOI: 10.1103/PhysRevLett.129.056801

Introduction.—While a universal fault-tolerant quantum computer with thousands of qubits remains elusive, noisy intermediate-scale quantum (NISQ) devices with a few qubits are already operational [1–3], albeit with limitations due to a lack of reliable error correction [4]. This progress has stirred a flurry of research activity to identify problems that can take advantage of this recently developed quantum technology [5]. Utilizing NISQ systems as digitized synthetic platforms to study physics phenomena challenging to investigate otherwise has emerged as a critical frontier [6].

In strongly correlated electron materials, fractional quantum Hall (FQH) states are widely studied for their exotic topological properties, such as excitations with fractional charge [7,8] and fractional statistics [9,10]. Recently, FQH states have come into focus due to their universal geometric features such as Hall viscosity [11–13] and the Girvin-MacDonald-Platzman magnetoroton collective mode [14,15]. In the long-wavelength limit $k \to 0$, the magnetoroton forms a quadrupole degree of freedom that carries angular momentum L=2 and can be represented by a quantum metric \tilde{g} [16]. For this reason, the $k \to 0$ limit of the magnetoroton has been referred to as "FOH

graviton" [17,18], due to its formal similarity with the fluctuating space-time metric in a theory of quantum gravity [19,20].

The experimental detection of the FQH graviton for $\nu = 1/3$ Laughlin state remains an outstanding challenge. While at large momenta, $k \sim \ell_B^{-1}$, with $\ell_B = \sqrt{\hbar/eB}$ being the magnetic length, the magnetoroton mode may be probed via inelastic light scattering [21-24], the magnetroroton enters the continuum near $k \to 0$ for the $\nu = 1/3$ Laughlin state (in contrast to the mode for $\nu = 7/3$ [25,26]). Haldane proposed that quantum-metric fluctuations can be exposed by breaking rotational symmetry [16]. Following up on this idea, recent theoretical works [27,28] have probed the FQH graviton by quenching the metric of "space," i.e., by suddenly making the FQH state anisotropic (see also alternative proposals [29-31]). It was found that such geometric quenches induce coherent dynamics of the FQH graviton [27], even though the graviton mode resides at finite energy densities above the FQH ground state. In contrast, near the FQH liquid-nematic phase transition [32,33], the graviton is expected to emerge as a gapless excitation [34–36].

In this Letter, we realize the FOH graviton in a synthetic NISQ system—the IBM open-access digitized quantum processor—and simulate its out-of-equilibrium dynamics. We first map the problem onto a one-dimensional quantum spin chain, corresponding to the FOH state on a thin cylinder (TC). While topological properties of FQH states have been extensively studied in this regime [37–44], we show that this limit remarkably captures some geometric properties of FQH systems, in particular, their quench dynamics. As a second step, we implement the quench dynamics on the IBM NISQ device, using two complementary approaches. On the one hand, we used an optimally compiled, noise-aware Trotterization circuit with error mitigation methods [45-47]. This allowed us to successfully simulate quench dynamics on the IBM device, overcoming the problem of the large circuit depth. On the other hand, we devised an efficient optimal-control-based [48–50] variational quantum algorithm [51–54], analogous to the quantum approximate optimization algorithm [55–59] that creates the postquench state using a hybrid classical-quantum approach [60,61]. We demonstrate that this method scales favorably with system size, with a linear-depth circuit depth and only two variational parameters. Some details are presented in the Supplemental Material [62].

Anisotropic Laughlin state near the thin-cylinder limit.— We focus on the $\nu=1/3$ Laughlin FQH state [7] whose Hamiltonian near the TC limit is given by [42]

$$\begin{split} \hat{H} &= \sum_{j} V_{1,0} \hat{n}_{j} \hat{n}_{j+1} + V_{2,0} \hat{n}_{j} \hat{n}_{j+2} + V_{3,0} \hat{n}_{j} \hat{n}_{j+3} \\ &+ V_{2,1} c_{j+1}^{\dagger} c_{j+2}^{\dagger} c_{j+3} c_{j} + \text{H.c.} \end{split} \tag{1}$$

Here the operators c_j , c_j^{\dagger} ($\hat{n}_j \equiv c_j^{\dagger} c_j$) destroy or create an electron in a Landau level orbital localized around $2\pi j \ell_B^2/L_2$. We assume the system is defined on a cylinder of size $L_1 \times L_2$ containing N electrons, such that the filling factor $\nu = N/N_{\phi} = 1/3$, with magnetic flux $N_{\phi} = (L_1 L_2)/(2\pi \ell_B^2)$. The near-TC limit corresponds to $L_1 \gg L_2$ with the area (N_{ϕ}) fixed, which allows us to neglect longer-range interaction terms beyond those in Eq. (1). Importantly, the Hamiltonian above describes a 2D system with strong spatial anisotropy, as opposed to a strictly 1D limit $L_2 \to 0$, thus allowing the emergence of the graviton mode. The interaction matrix elements are given by

$$V_{k,m} = (k^2 - m^2)e^{-2\pi^2(k^2 + m^2 - 2ikmg_{12})/L_2^2g_{11}}, \qquad (2)$$

which we have generalized to the case of an arbitrary electron mass tensor g_{ab} , a, b=1, 2. The mass tensor must be symmetric and unimodular (det g=1) [16]; hence we can generally write it as $g=\exp(\hat{Q})$, where $\hat{Q}=Q(2\hat{d}_a\hat{d}_b-\delta_{a,b})$ is a Landau-de Gennes order parameter

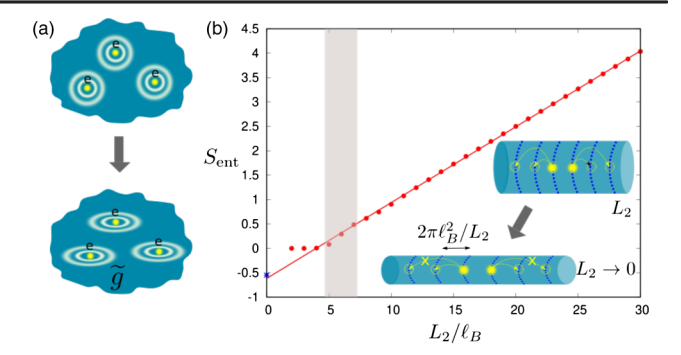


FIG. 1. (a) Geometric quench probes the fluctuations of the quantum metric \tilde{g} [16]. (b) Entanglement entropy $S_{\rm ent}$ for the $\nu=1/3$ Laughlin state on a cylinder as a function of the circumference L_2 . Entropy obeys the area law for sufficiently large circumferences $L_2\gtrsim 5\ell_B$, with a subleading correction close to the expected value $-\ln(3)/2$ (blue star). Data are obtained using the matrix product method [70,71] with entanglement truncation $P_{\rm max}=18$. Near the thin-cylinder limit (shaded), long-range electron hopping becomes strongly suppressed, as shown in the inset.

and $\hat{\mathbf{d}} = [\cos(\phi/2), \sin(\phi/2)]$ is a unit vector [69]. Parameters Q and ϕ intuitively represent the stretch and rotation of the metric, respectively. The FQH state is invariant under area-preserving deformations of g, illustrated in Fig. 1(a).

Since the Hamiltonian in Eq. (1) is positive semidefinite, it has a unique (unnormalized) ground state with zero energy [42],

$$|\psi_{0}\rangle = \prod_{j} \left(1 - \sqrt{\frac{V_{3,0}}{V_{1,0}}} e^{i(8\pi^{2}\ell_{B}^{2}/L_{2}^{2})(g_{12}/g_{11})} \hat{S}_{j} \right) | \dots 100100 \dots \rangle,$$
(3)

where $\hat{S}_j = c_{j+1}^{\dagger} c_{j+2}^{\dagger} c_{j+3} c_j$ is an operator that "squeezes" two neighboring electrons while preserving their center-of-mass position [72]. The ground state in the limit $L_2 \to 0$ is the product state $|...100100...\rangle$. The off-diagonal squeezing operator is essential for the 1/3 Laughlin state [37].

In previous works [37,42–44], the ground state of the model in Eq. (1) and its neutral excitations were studied on isotropic cylinders, $g_{11} = g_{22} = 1$, $g_{12} = 0$. In particular, it was found that the state in Eq. (3) has ~98% overlap with the ground state of the full Hamiltonian in the range of circumferences $5\ell_B \lesssim L_2 \lesssim 7\ell_B$, where $V_{2,1}/V_{1,0} \approx 0.2$ –0.3, justifying the use of the truncated model Eq. (1) in this regime [42]. We have confirmed that the same conclusions continue to hold in the presence of mass anisotropy [62].

As a further justification of the model in Eq. (1), we plot the entanglement entropy $S_{\rm ent}$ of the Laughlin state in a large system of 100 electrons as a function of the circumference L_2 in Fig. 1(b). We see that it is possible to reduce

 L_2 to approximately $5\ell_B$, where the "area law" for entanglement entropy [73,74] still holds, but long-range electron hopping is strongly suppressed. Below, we focus on this regime, where the key aspects of 2D physics are preserved, but the system can be mapped to a 1D spin chain model and thus efficiently simulated on quantum hardware.

Geometric quench.—We now show that, in addition to the ground state, the effective model in Eq. (1) captures the high-energy excitations that govern the graviton dynamics in the FQH phase. We initially prepare the system in the ground state $|\psi_0\rangle$ in Eq. (3) with isotropic metric $(g_{11}=g_{22}=1,\,g_{12}=0)$. At time t=0, we instantaneously introduce diagonal anisotropy, $g'_{11}=1/g'_{22}>1$, and let the system evolve unitarily, under the dynamics generated by the postquench anisotropic Hamiltonian. We are interested in the dynamical fluctuations of its quantum metric \tilde{g} as the system is taken out of equilibrium.

Note that even though g and \tilde{g} are related to one another, \tilde{g} is an emergent property of a many-body state and not necessarily equal to g. Nevertheless, we can formally parametrize \tilde{g} using the parameters \tilde{Q} and $\tilde{\phi}$, representing the stretch and rotation of the emergent metric. In order to determine the equations of motion for \tilde{Q} and $\tilde{\phi}$, we maximize the overlap between $|\psi(t)\rangle$ and the family of trial states in Eq. (3) [75]. When this overlap is close to unity, we can be confident that we found the optimal metric parameters \tilde{Q} and $\tilde{\phi}$ describing the state $|\psi(t)\rangle$.

In Fig. 2, we summarize the results of the graviton dynamics in the model in Eq. (1) when anisotropy is suddenly changed from Q=0 to $Q\approx 0.18$ while keeping $\phi=0$. Figure 2(a) shows the dynamics of \tilde{Q} and $\tilde{\phi}$ for different system sizes N. The dynamics is in excellent agreement with the bimetric theory in the linear regime [76],

$$\tilde{Q}(t) = \pm 2A \sin \frac{E_g t}{2}, \qquad \tilde{\phi}(t) = \pm \frac{\pi}{2} - \frac{E_g t}{2}, \quad (4)$$

where E_g is the energy of the graviton mode in units of $V_{1,0}$. As can be seen in Fig. 2(a), the numerical data can be accurately fitted using Eqs. (4). The fit yields the oscillation frequency $E_g=1.29$. Note that this energy is much higher than the first excited energy of the quench Hamiltonian. We identify this energy with the graviton state as evidenced by the sharp peak in the quadrupole (L=2) spectral function $I_{1,2}(\omega)$ [77]. The later spectral function is designed to detect the characteristic d-wave symmetry of the graviton. Analogous to an oscillating space-time metric induced by a gravitational wave, $I_{1,2}(\omega)$ is the associated transition rate due to the dynamics of the oscillating mass tensor [77]. Thus, the model in Eq. (1) reproduces the graviton oscillation as described by the bimetric theory.

Spin-chain mapping.—We use the reduced registers scheme introduced in Ref. [41] to map the model (1) to a spin chain; see also Ref. [62] for further details. The reduced register is a block of three consecutive orbitals that

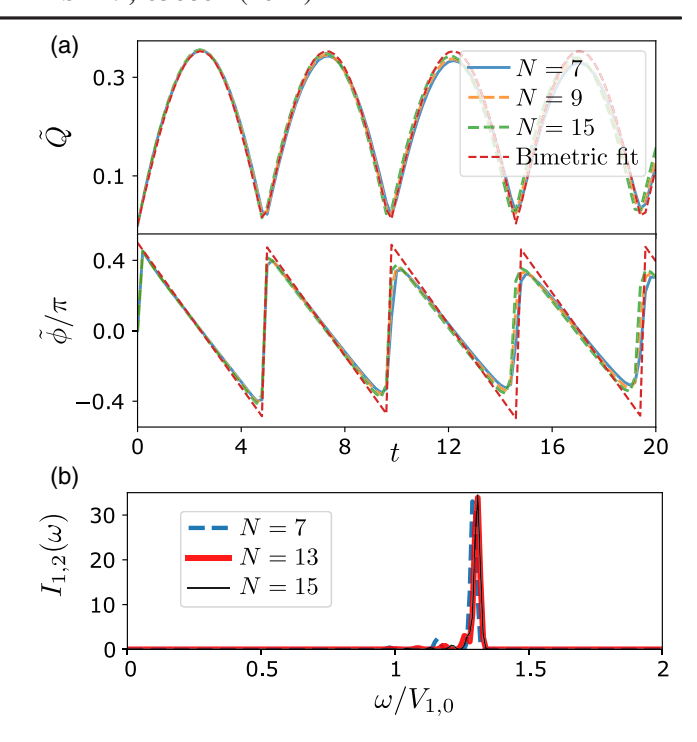


FIG. 2. (a) Dynamics of \tilde{Q} and $\tilde{\phi}$ following the geometric quench in the TC limit, with $L_2 = 5.477\ell_B$ and postquench anisotropy $Q \approx 0.18$. Data are for system sizes N = 7, 9, 15 electrons. (b) Quadrupole spectral function $I_{1,2}$ shows a sharp peak at the graviton energy $E_g \approx 1.29$, which agrees well with the frequency of the oscillations in (a).

encodes whether or not the block is squeezed with respect to the root state $|100, 100, ...\rangle$. For each block of three sites, the state of the reduced register is 1 if it is squeezed (i.e., 011) or 0 if not (i.e., either 000 or 100). In the root state, none of the blocks are squeezed and it maps to $[0, 0, 0, ...\rangle$. If we apply the squeezing operator to one block of the root state, we obtain, e.g., $|100,011,000,...\rangle \rightarrow |0,1,0,...\rangle$. In terms of reduced registers, squeezing acts as flip of 0 to 1, so it can be viewed as the Pauli X matrix. However, there is an important difference in that the Hilbert space is not a tensor product of reduced registers, since the squeezing can never generate two neighboring ...11... configurations of the reduced registers [63,78]. This type of constrained Hilbert space arises, e.g., in the Fibonacci anyon chain [79]. The inverse mapping is constructed as follows: for any 1 we make a 011 block. A 0 that follows a 1 (0) gives a 000 (100) block. With this mapping of states, we can show that the Hamiltonian (1) maps to a local spin-chain Hamiltonian,

$$\begin{split} \hat{H} &= \sum_{\ell} \{ (V_{1,0} - 3V_{3,0}) \mathcal{N}_{\ell} + V_{3,0} \mathcal{N}_{\ell} \mathcal{N}_{\ell+2} \\ &+ (1 - \mathcal{N}_{\ell-1}) [\text{Re}(V_{2,1}) X_{\ell} - \text{Im}(V_{2,1}) Y_{\ell}] (1 - \mathcal{N}_{\ell+1}) \}, \end{split}$$

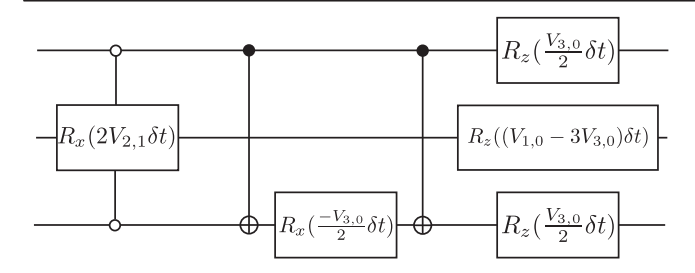


FIG. 3. Circuit implementation of the Trotterized unitary U_{ℓ} in the bulk of the spin chain.

where we omitted the boundary terms for simplicity and introduced the occupation number $\mathcal{N} \equiv |\mathbb{1}\rangle\langle\mathbb{1}|$, Pauli $X \equiv |\mathbb{0}\rangle\langle\mathbb{1}| + |\mathbb{1}\rangle\langle\mathbb{0}|$, and Pauli $Y \equiv -i|\mathbb{0}\rangle\langle\mathbb{1}| + i|\mathbb{1}\rangle\langle\mathbb{0}|$ operators.

Quantum simulation.—The standard procedure for simulating the time evolution $e^{-i\hat{H}t}$ is to use Trotter decomposition. Here \hat{H} is given in Eq. (5) with real $V_{2,1}$ and it has the form $\hat{H} = \sum_{\ell} H_{\ell}$. We decompose the evolution operator into k Trotter steps as $e^{-i\hat{H}t} \approx [\prod_{l} U_{\ell}(t/k)]^{k}$, where $\delta t = t/k$ and the approximation improves for larger k [80]. In Ref. [62], we derive the circuit which implements a Trotterized time evolution of our Hamiltonian, and the subcircuit for the bulk $U_{\ell}(\delta t)$ is shown in Fig. 3. Below, we demonstrate that this circuit yields good results on current IBM devices with 5 qubits after using noise-aware error mitigation methods and optimized compilations [45–47].

While the Trotterization algorithm emulates the actual quantum evolution resulting from FQH quenched Hamiltonian, it has a relatively large number of entangling gates. We can access large systems by a hybrid classical-quantum method that requires classical optimization, using the following variational ansatz for the final postquench state $|\psi(t)\rangle$:

$$|\psi_{\text{var}}(\alpha,\beta)\rangle = \prod_{\ell} e^{-i\alpha\mathcal{N}_{\ell}} e^{-i\beta(1-\mathcal{N}_{\ell-1})X_{\ell}} |\mathbb{OOO...}\rangle, \quad (6)$$

where on each reduced register ℓ we apply alternating gates \mathcal{N}_{ℓ} and $[1-\mathcal{N}_{\ell-1})X_{\ell}$ (on the very first site, due to open boundary condition, we use X_1 instead of $(1-\mathcal{N}_{\ell-1})X_{\ell}$ for $\ell=1$].

The optimal parameters α^* , $\beta^* \in [0, 2\pi)$ are determined at each time step t using classical optimization by the dual annealing algorithm to maximize the overlap $|\langle \psi_0|U^\dagger(t)|\psi_{\text{var}}(\alpha,\beta)\rangle|$ with the exact state. Naively, it appears that the classical optimization needs to be performed for each t and system size. Importantly, however, we find the optimal parameters α^* , β^* to exhibit a simple oscillatory behavior as a function of time, as well as weak dependence on the system size as shown in Figs. 4(a) and 4(b). The data for system sizes $N=7,\ldots,13$ almost collapse, allowing a smooth extrapolation to the thermodynamic limit $(N\to\infty)$, shown as the solid black line.

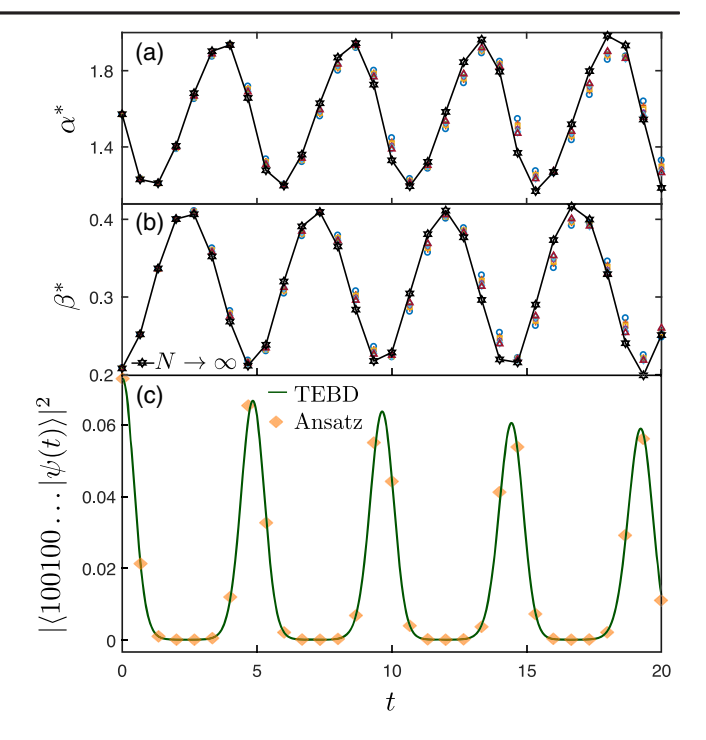


FIG. 4. (a), (b) Optimal variational parameters α^* and β^* for N=7–13 particles and their extrapolation to $N\to\infty$ (solid black line). Optimal parameters vary smoothly with time and exhibit weak finite-size effects. (c) Comparison of the variational ansatz against TEBD simulation for N=60 for the overlap of the time-evolved state with the root state. The parameters of the variational ansatz are extrapolated to the same system size, N=60. The ansatz with extrapolated parameters exhibits excellent agreement with the TEBD results. TEBD simulations were performed using a bond dimension 20 with a time step $\Delta t=0.01$, resulting in truncation error 10^{-5} .

In Fig. 4(c), we have checked using time-evolved block decimation (TEBD) [81] that the extrapolated parameters produce excellent agreement with direct TEBD calculation of $|\psi(t)\rangle$ for larger systems. Thus, the weak system-size dependence of the variational parameters eliminates the need to directly perform the classical optimization for the actual size of the system, providing access to system sizes for which the classical optimization is infeasible.

Our variational algorithm's circuit depth scales as the number of qubits N independent of the evolution time t. As for Trotterization, since we have a local lattice model in one dimension with no explicit Hamiltonian time dependence, the total circuit depth is expected to scale as Nt for a fixed error tolerance [82,83]. Despite higher complexity, Trotterization corresponds to the actual unitary operator describing the quantum evolution and does not need any classical optimization or variational ansatz. Both algorithms have good scalability potential to more qubits.

Results on the IBM quantum processor.—In Fig. 5, we present our measurements of the root state fidelity $|\langle \psi(t)\rangle| |100100.....\rangle|^2$, the local density $\langle n_i\rangle$ and the

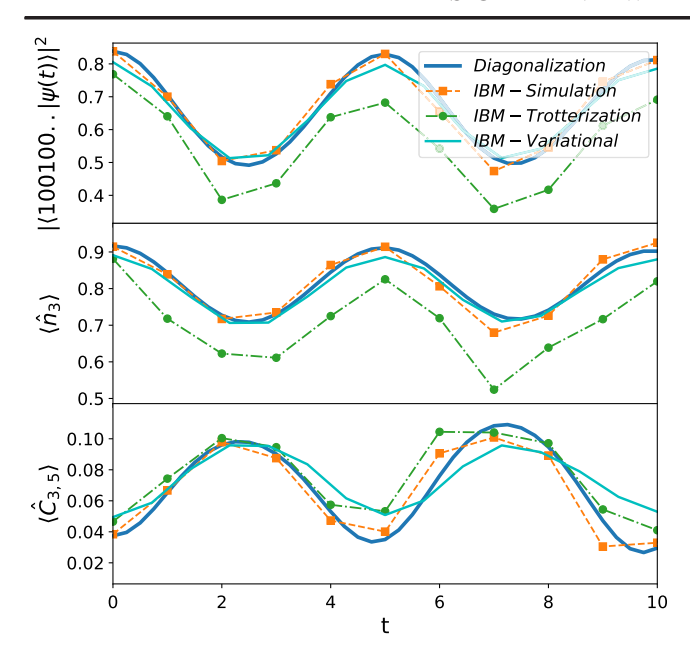


FIG. 5. N=5 quench results for the time dependence of fidelity, density, and correlation function. Comparison between exact diagonalization results, k=15 depth Trotterization circuit on the IBM simulator, gate optimized unitary output from IBM-Perth, and variational ansatz results from IBM-Santiago. The dynamics were simulated on IBM-Perth on January 7, 2022 and on IBM-Santiago on June 12, 2021.

equal-time density-density correlation function $C_{i,j}(t) = -\langle n_i(t)n_j(t)\rangle + \langle n_i(t)\rangle\langle n_j(t)\rangle$. While these quantities are in terms of the original fermionic basis, they are easily extracted from measurements in the reduced basis using the rules discussed above Eq. (5). As shown in Fig. 5, the variational results are in excellent agreement with the simulations. Similarly, the error-mitigated Trotter algorithm faithfully generates oscillations with the expected graviton frequency despite deeper circuits and higher execution-time error rates than the variational algorithm, which only induce quantitative shifts.

We note that the noise levels of the IBM devices vary widely. Using Qiskit library, we executed error-mitigated circuit for the Trottrization algorithm on ibmq_perth processor [84] with readout error, CNOT noise, and T2 dephasing time of roughly 1.4%, 1.7%, and 109 μ s, respectively. The variational ansatz was executed on IBM's ibmq_santiago processor [84] with averaged readout error, CNOT noise, and T2 dephasing time of roughly 1.5%, 0.6%, and 120 μ s, respectively. We also performed simulations of our circuits in Qiskit for comparison. Using postselection methods, we improve the measurements by discarding states that lie outside the physical Hilbert space.

Conclusions.—We showed that quantum-geometrical features of FQH states can be realized in an effective 1D model that has an efficient quantum-circuit representation. Our 1D model makes efficient use of resources, as each

qubit corresponds to three Landau orbitals, reminiscent of holographic quantum simulation [85]. As a proof of principle, utilizing the quantum-circuit mapping, we developed efficient quantum algorithms that allowed us to simulate graviton dynamics on IBM quantum processors. We used state-of-the-art error mitigation to successfully run the deep Trotterization circuit, which does not require any classical optimization. We also developed a variational algorithm with a linear circuit depth (independent of the evolution time), which makes use of classical optimization but can be scaled to the thermodynamic limit, similar to approaches based on infinite matrix-product states [86–89]. We expect these results will motivate further analytical investigations into tractable models of graviton dynamics in condensed matter systems, as well as their realizations on NISO devices.

In compliance with EPSRC policy framework on research data, this publication is theoretical work that does not require supporting research data.

We thank Areg Ghazaryan and Zhao Liu for useful comments. We acknowledge the use of IBM Quantum services for this work. The views expressed are those of the authors, and do not reflect the official policy or position of IBM or the IBM Quantum team. A. K. is supported by Grants No. DMR-2037996 and No. DMR-2038028. P. G. acknowledges support from NSF Awards No. DMR-2037996 and No. DMR-1824265. A. R. acknowledges support from NSF Awards No. DMR-1945395 and No. DMR-2038028. A. R. and Z. P. thank the Kavli Institute for Theoretical Physics, acknowledging support by the NSF under Grant No. PHY1748958. Z. P. and K. B. acknowledge support by EPSRC Grants No. EP/R020612/1 and No. EP/M50807X/1, and by the Leverhulme Trust Research Leadership Award No. RL-2019-015.

^[1] F. Arute et al., Nature (London) **574**, 505 (2019).

^[2] S. Boixo, S. V. Isakov, V. N. Smelyanskiy, R. Babbush, N. Ding, Z. Jiang, M. J. Bremner, J. M. Martinis, and H. Neven, Nat. Phys. 14, 595 (2018).

^[3] C. Neill et al., Nature (London) 594, 508 (2021).

^[4] J. R. Wootton, Quantum Sci. Technol. 5, 044004 (2020).

^[5] K. Bharti et al., Rev. Mod. Phys. 94, 015004 (2022).

^[6] Z. Jiang, K. J. Sung, K. Kechedzhi, V. N. Smelyanskiy, and S. Boixo, Phys. Rev. Applied **9**, 044036 (2018).

^[7] R. B. Laughlin, Phys. Rev. Lett. **50**, 1395 (1983).

^[8] R. de Picciotto, M. Reznikov, M. Heiblum, V. Umansky, G. Bunin, and D. Mahalu, Nature (London) 389, 162 (1997).

^[9] J. Nakamura, S. Liang, G. C. Gardner, and M. J. Manfra, Nat. Phys. 16, 931 (2020).

^[10] H. Bartolomei, M. Kumar, R. Bisognin, A. Marguerite, J.-M. Berroir, E. Bocquillon, B. Plaçais, A. Cavanna, Q. Dong, U. Gennser, Y. Jin, and G. Fève, Science 368, 173 (2020).

- [11] J. E. Avron, R. Seiler, and P. G. Zograf, Phys. Rev. Lett. 75, 697 (1995).
- [12] N. Read, Phys. Rev. B 79, 045308 (2009).
- [13] F. D. M. Haldane, arXiv:0906.1854.
- [14] S. M. Girvin, A. H. MacDonald, and P. M. Platzman, Phys. Rev. Lett. 54, 581 (1985).
- [15] S. M. Girvin, A. H. MacDonald, and P. M. Platzman, Phys. Rev. B 33, 2481 (1986).
- [16] F. D. M. Haldane, Phys. Rev. Lett. 107, 116801 (2011).
- [17] B. Yang, Z.-X. Hu, Z. Papić, and F. D. M. Haldane, Phys. Rev. Lett. 108, 256807 (2012).
- [18] S. Golkar, D. X. Nguyen, and D. T. Son, J. High Energy Phys. 01 (2016) 021.
- [19] E. A. Bergshoeff, S. de Haan, O. Hohm, W. Merbis, and P. K. Townsend, Phys. Rev. Lett. 111, 111102 (2013).
- [20] E. A. Bergshoeff, J. Rosseel, and P. K. Townsend, Phys. Rev. Lett. 120, 141601 (2018).
- [21] A. Pinczuk, B. S. Dennis, L. N. Pfeiffer, and K. West, Phys. Rev. Lett. 70, 3983 (1993).
- [22] P. M. Platzman and S. He, Phys. Scr. T66, 167 (1996).
- [23] M. Kang, A. Pinczuk, B. S. Dennis, L. N. Pfeiffer, and K. W. West, Phys. Rev. Lett. 86, 2637 (2001).
- [24] I. V. Kukushkin, J. H. Smet, V. W. Scarola, V. Umansky, and K. von Klitzing, Science 324, 1044 (2009).
- [25] U. Wurstbauer, A. L. Levy, A. Pinczuk, K. W. West, L. N. Pfeiffer, M. J. Manfra, G. C. Gardner, and J. D. Watson, Phys. Rev. B 92, 241407(R) (2015).
- [26] T. Jolicoeur, Phys. Rev. B 95, 075201 (2017).
- [27] Z. Liu, A. Gromov, and Z. Papić, Phys. Rev. B 98, 155140 (2018).
- [28] M. F. Lapa, A. Gromov, and T. L. Hughes, Phys. Rev. B 99, 075115 (2019).
- [29] S.-F. Liou, F.D.M. Haldane, K. Yang, and E.H. Rezayi, Phys. Rev. Lett. **123**, 146801 (2019).
- [30] D. X. Nguyen and D. T. Son, Phys. Rev. Research 3, 023040 (2021).
- [31] Y. Wang and B. Yang, Phys. Rev. B 105, 035144 (2022).
- [32] J. Xia, J. P. Eisenstein, L. N. Pfeiffer, and K. W. West, Nat. Phys. 7, 845 (2011).
- [33] N. Samkharadze, K. A. Schreiber, G. C. Gardner, M. J. Manfra, E. Fradkin, and G. A. Csáthy, Nat. Phys. 12, 191 (2016).
- [34] N. Regnault, J. Maciejko, S. A. Kivelson, and S. L. Sondhi, Phys. Rev. B 96, 035150 (2017).
- [35] Y. You, G. Y. Cho, and E. Fradkin, Phys. Rev. X 4, 041050 (2014).
- [36] B. Yang, Phys. Rev. Research 2, 033362 (2020).
- [37] E. H. Rezayi and F. D. M. Haldane, Phys. Rev. B **50**, 17199 (1994).
- [38] E. J. Bergholtz and A. Karlhede, Phys. Rev. Lett. **94**, 026802 (2005).
- [39] A. Seidel, H. Fu, D.-H. Lee, J. M. Leinaas, and J. Moore, Phys. Rev. Lett. 95, 266405 (2005).
- [40] E. J. Bergholtz and A. Karlhede, Phys. Rev. B 77, 155308 (2008).
- [41] A. Rahmani, K. J. Sung, H. Putterman, P. Roushan, P. Ghaemi, and Z. Jiang, PRX Quantum 1, 020309 (2020).
- [42] M. Nakamura, Z.-Y. Wang, and E. J. Bergholtz, Phys. Rev. Lett. 109, 016401 (2012).
- [43] Z.-Y. Wang and M. Nakamura, Phys. Rev. B 87, 245119 (2013).

- [44] P. Soulé and T. Jolicoeur, Phys. Rev. B 85, 155116 (2012).
- [45] V. Saravanan and S. M. Saeed, IEEE Trans. Quantum Eng. 3, 1 (2022).
- [46] H. Abraham *et al.*, Qiskit: An open-source framework for quantum computing (2019), https://zenodo.org/record/2562111#.Ys2MbITMI2w.
- [47] M. G. Davis, E. Smith, A. Tudor, K. Sen, I. Siddiqi, and C. Iancu, in *Proceedings of the 2020 IEEE International Conference on Quantum Computing and Engineering (QCE)* (IEEE, Piscataway, NJ, 2020), pp. 223–234.
- [48] J. Werschnik and E. K. U. Gross, arXiv:0707.1883.
- [49] I. Petersen and D. Dong, IET Control Theory Appl. 4, 2651 (2010).
- [50] A. Rahmani, Mod. Phys. Lett. B 27, 1330019 (2013).
- [51] A. Peruzzo, J. McClean, P. Shadbolt, M. H. Yung, X. Q. Zhou, P. J. Love, A. Aspuru-Guzik, and J. L. O'Brien, Nat. Commun. 5, 4213 (2014).
- [52] D. Wecker, M. B. Hastings, and M. Troyer, Phys. Rev. A 92, 042303 (2015).
- [53] D. Wecker, M. B. Hastings, and M. Troyer, Phys. Rev. A 94, 022309 (2016).
- [54] J. R. McClean, J. Romero, R. Babbush, and A. Aspuru-Guzik, New J. Phys. 18, 023023 (2016).
- [55] E. Farhi, J. Goldstone, and S. Gutmann, arXiv:1411.4028.
- [56] E. Farhi and A. W. Harrow, arXiv:1602.07674.
- [57] Z.-C. Yang, A. Rahmani, A. Shabani, H. Neven, and C. Chamon, Phys. Rev. X 7, 021027 (2017).
- [58] Z. Wang, S. Hadfield, Z. Jiang, and E. G. Rieffel, Phys. Rev. A 97, 022304 (2018).
- [59] L. Zhou, S.-T. Wang, S. Choi, H. Pichler, and M. D. Lukin, Phys. Rev. X 10, 021067 (2020).
- [60] C. Kokail, C. Maier, R. van Bijnen, T. Brydges, M. K. Joshi, P. Jurcevic, C. A. Muschik, P. Silvi, R. Blatt, C. F. Roos, and P. Zoller, Nature (London) 569, 355 (2019).
- [61] A. Kandala, A. Mezzacapo, K. Temme, M. Takita, M. Brink, J. M. Chow, and J. M. Gambetta, Nature (London) **549**, 242 (2017).
- [62] See Supplemental Material at http://link.aps.org/supplemental/10.1103/PhysRevLett.129.056801 for the details of the Hamiltonian and spin-chain model derivation, graviton excitations near the thin-torus limit, geometric quench and the limitations of the bimetric theory, the Trotterization circuit and error mitigation methods, which includes Refs. [63–68].
- [63] S. Moudgalya, A. Prem, R. Nandkishore, N. Regnault, and B. A. Bernevig, Thermalization and its absence within Krylov subspaces of a constrained hamiltonian, in *Memorial Volume for Shoucheng Zhang* (World Scientific, Singapore, 2021), pp. 147–209.
- [64] Z. Papić, Phys. Rev. B 87, 245315 (2013).
- [65] B. Yang, C. H. Lee, C. Zhang, and Z.-X. Hu, Phys. Rev. B 96, 195140 (2017).
- [66] S. Carroll and S. Carroll, *Spacetime and Geometry: An Introduction to General Relativity* (Addison Wesley, Reading, MA, 2004).
- [67] X. G. Wen and A. Zee, Phys. Rev. Lett. 69, 953 (1992).
- [68] Y. Nam, N. J. Ross, Y. Su, A. M. Childs, and D. Maslov, npj Quantum Inf. 4, 23 (2018).
- [69] J. Maciejko, B. Hsu, S. A. Kivelson, Y. J. Park, and S. L. Sondhi, Phys. Rev. B 88, 125137 (2013).

- [70] M. P. Zaletel and R. S. K. Mong, Phys. Rev. B 86, 245305 (2012).
- [71] B. Estienne, Z. Papić, N. Regnault, and B. A. Bernevig, Phys. Rev. B 87, 161112(R) (2013).
- [72] B. A. Bernevig and F. D. M. Haldane, Phys. Rev. Lett. 100, 246802 (2008).
- [73] A. Kitaev and J. Preskill, Phys. Rev. Lett. **96**, 110404 (2006).
- [74] M. Levin and X.-G. Wen, Phys. Rev. Lett. 96, 110405 (2006).
- [75] B. Yang, Z. Papić, E. H. Rezayi, R. N. Bhatt, and F. D. M. Haldane, Phys. Rev. B 85, 165318 (2012).
- [76] A. Gromov and D. T. Son, Phys. Rev. X 7, 041032 (2017).
- [77] K. Yang, Phys. Rev. B 93, 161302(R) (2016).
- [78] S. Moudgalya, B. A. Bernevig, and N. Regnault, Phys. Rev. B 102, 195150 (2020).
- [79] A. Feiguin, S. Trebst, A. W. W. Ludwig, M. Troyer, A. Kitaev, Z. Wang, and M. H. Freedman, Phys. Rev. Lett. 98, 160409 (2007).
- [80] A. Smith, M. S. Kim, F. Pollmann, and J. Knolle, npj Quantum Inf. 5, 106 (2019).

- [81] G. Vidal, Phys. Rev. Lett. 93, 040502 (2004).
- [82] J. Haah, M. B. Hastings, R. Kothari, and G. H. Low, SIAM J. Comput. FOCS18 (2021).10.1137/18M1231511
- [83] A. M. Childs, Y. Su, M. C. Tran, N. Wiebe, and S. Zhu, Phys. Rev. X 11, 011020 (2021).
- [84] IBM Quantum, https://quantum-computing.ibm.com, 2021.
- [85] M. Foss-Feig, D. Hayes, J. M. Dreiling, C. Figgatt, J. P. Gaebler, S. A. Moses, J. M. Pino, and A. C. Potter, Phys. Rev. Research 3, 033002 (2021).
- [86] S.-H. Lin, R. Dilip, A. G. Green, A. Smith, and F. Pollmann, PRX Quantum 2, 010342 (2021).
- [87] F. Barratt, J. Dborin, M. Bal, V. Stojevic, F. Pollmann, and A. G. Green, npj Quant. Inform. 7, 79 (2021).
- [88] M. Foss-Feig, S. Ragole, A. Potter, J. Dreiling, C. Figgatt, J. Gaebler, A. Hall, S. Moses, J. Pino, B. Spaun et al., Phys. Rev. Lett. 128, 150504 (2022).
- [89] A. Smith, B. Jobst, A. G. Green, and F. Pollmann, Phys. Rev. Research 4, L022020 (2022).